This is the post print version of the article, which has been published in Macromolecular bioscience . 2018, 18 (10),1800094.https://doi.org/10.1002/mabi.201800094.

Reactive Self-assembly and Specific Cellular Delivery of NCO-sP(EO-stat-PO) Derived Nanogels

Haika Hildebrandt[1], Outi Paloheimo[2], Elina Mäntylä[3], Sami Willman[3], Satu Hakanen[3], Krystyna Albrecht[4], Jürgen Groll[4], Martin Möller[1*] and Maija Vihinen-Ranta[3*]

[1] Institute of Technical and Macromolecular Chemistry and DWI - Leibniz Institute for Interactive Materials, RWTH Aachen University, Forckenbeckstraße 50, 52056 Aachen, Germany
[2]BioMediTech and Faculty of Medicine and Life Sciences, University of Tampere, Arvo Ylpön katu 34, FI-33520 Tampere, Finland
[3] Department of Biological and Environmental Science, and Nanoscience Center, University of Jyvaskyla, Survontie 9, FI-40500, Jyvaskyla, Finland
[4] Department of Functional Materials in Medicine and Dentistry and Bavarian Polymer Institute (BPI), University of Würzburg, Pleicherwall 2, 97070 Würzburg, Germany

[*]Corresponding authors, E-mail: moeller@dwi.rwth-aachen.de; E-mail: maija.vihinen-ranta@jyu.fi

Running Title: Reactive self-assembly and cell uptake of nanogels

Key words: Nanogel, reactive self-assembly, cellular entry

Abstract

This study presents the reactive self-assembly of isocyanate functional and amphiphilic six-arm star-shaped polyether prepolymers in water into nanogels. Intrinsic molecular amphiphilicity, mainly driven by the isophorone moiety at the distal endings of the star-shaped molecules allowed for the preparation of spherical particles with an adjustable size of 100-200 nm by self-assembly and subsequent covalent cross-linking without the need for organic solvents or tensides. Covalent attachment of a fluorescence dye and either the cell-penetrating TAT peptide or a random control peptide sequence showed that only TAT labeled nanogels are internalized by HeLa cells. The nanogels thus specifically entered the cells and accumulated in the perinuclear area in a time- and concentration-dependent manner.

Table of Contents:

We describe the organic solvent and tenside-free reactive self-assembly of isocyanate functional amphiphilic star-shaped prepolymers into nanogels that can be loaded with hydrophobic guest molecules. Furthermore, modification with cell-penetrating peptides facilitates the cellular uptake of these nanogels.

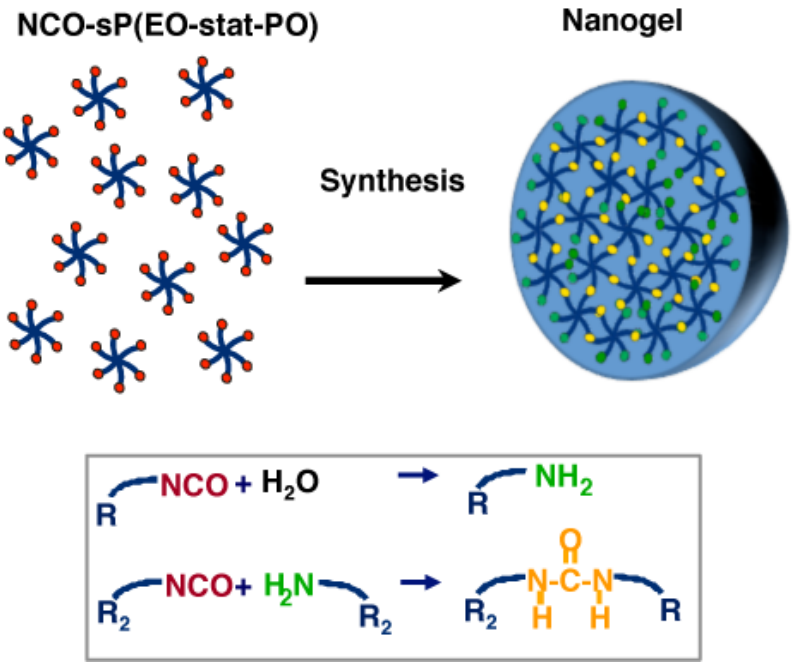

1 Introduction

Nanogels have attracted increasing interest in recent years, especially for biomedical applications (Hamidi et al 2008; Chacko et al. 2012). They are colloidal hydrogels that, by definition, consist of a three-dimensionally cross-linked hydrophilic polymer network, have sub-micrometer diameter, and swell significantly without being dissolved in water (Kabanov et al. 2009,Vinogradov et al. 1999). Nanogels thus combine the unique characteristics of nanoparticles and bulk hydrogels, such as softness, high water content and low interfacial tension with water and biological fluids, as well as intrinsic cytocompatibility (Krsko et al 2005). Their open porous network structure allows the transport and diffusion of small molecules, while the large surface-to-volume ratio enables interactions with cells and proteins on a molecular level (Yallapu, et al. 2011, Li et al. 2015). Notably, nanogels can reach high loading and entrapment efficiencies for guest molecules (Ryu et al. 2010, Kettel et. al., 2012), which makes them equally interesting for use as coating components with sustained release (Kettel et al. 2015), for sequestration of pollutants and toxins (Topuz et. al., 2015) as well as for drug delivery purposes, where they potentially enable a reduction of doses needed for therapeutic delivery (Wu et al. 2016). A common method for testing the drug loading capacity of nanoparticles is to load them with fluorescent hydrophobic pyrene and examine the solvatochromic effect. (Chen et al. 2009).

A promising strategy for enhancing the cellular uptake of nanoparticles is the attachment of cell-penetrating peptides to their surface (Janver et al. 2004, Field et al. 2015, Petros et al. 2010, Vasir et al. 2005). One of the best-studied efficient peptides is formed from 11aminoacids of the human immunodeficiency virus type 1 (HIV-1) TAT protein. The basic region of TAT, containing amino acid residues 47-57 (YGRKKRRQRRR; TAT_{47-57}) is crucial for many key functions of the viral life cycle, including cellular entry and nuclear import (Lewin, et al. 2005, Nitin et al 2009, Pan 2012). TAT_{47-57} has been used for intracellular delivery of diverse cargo, including liposomes, micelles and nanoparticles (Roosmarijn et al. 2007). Both unconjugated

TAT peptide and TAT-conjugated nanoparticles are internalized into cells by clathrin-dependent endocytosis or by macropinocytosis (Mann & Frankel 1991, Richard et al. 2005, Kaplan et al. 2005).

For traditional solid nanoparticles, it is often necessary to reduce non-specific binding and enhance the specificity of peptide-mediated cellular uptake bycoating the nanoparticles with a layer (typically consisting of hydrophilic polymer chains,) that minimizes interactions. The most successful approach is the introduction of multiple poly (ethylene glycol) (PEG) molecules onto the nanoparticle surface (Choi et al. 2007). PEG is non-immunogenic and non-antigenic, and it has been approved for clinical use by the Food and Drug Administration (FDA). In the case of nanogels, an extra surface coating is not necessary, as the nanogels themselves consist of hydrophilic polymer chains and lack a primary phase boundary. However,, nanogel preparation often involves the use of tensides or water emulsions with organic solvents that need to be removed from the final product. Radically polymerized disulfide-functional polyacrylates with oligoethyleneglycol side chains for hydrophilicity have been used to form nanogels in an emulsion-free process (Ryu et al. 2010). We reported before that reactive star-shaped prepolymers with a sorbitol core and a statistically copolymerized backbone of 80% ethylene oxide and 20% propylene oxide that have been endowed with isocyanate groups at the distal endings of the arms (NCO-sP(EO-stat-PO) can be used to prepare nanogels without using tensides or solvents(Kettel et al. 2012; Kettel et al. 2015). In these studies, however, cyclodextrins were used as a multifunctional nucleating agent that also served as a depot for guest molecules for the preparation of sustained release from textile coatings.

Here we demonstrate that sP(EO-stat-PO) molecules are intrinsically sufficiently amphiphilic to form nanogels through reactive self-assembly even without a nucleating agent. This process occurs spontaneously in water in a concentration-dependent manner, and can be used to generate nanogels that chemically cross-link after the assembly through isocyanate hydrolysis,which is

followed by intermolecular cross-linking of the resulting amines with isocyanate groups, forming urea bridges. We optimized the protocol to produce stable particles within the size range of 100-250 nm as characterized by dynamic light scattering (DLS), cryo-scanning (cryo-SEM) and transmission electron microscopy analyses (TEM). Next, we used pyrene to demonstrate that hydrophilic guest molecules can be loaded into these nanogels, which we evaluated using fluorescence spectroscopy. Finally, we demonstrate that these nanogels can be covalently functionalized with amino-functional fluorescence dyes and peptide sequences by simple mixing of those compounds in the nanogel preparation mixture. Using an amine functional Alexa-Fluor derivative with the TAT peptide sequence or a randomized control peptide sequence, we demonstrate that unmodified nanogels and nanogels with the control peptide sequence are only marginally taken up by cells, whereas the TAT-labeled nanogels are rapidly internalized by HeLa cells as confirmed by confocal microscopy imaging and flow cytometry analysis.

2 Experimental Section

2.1 Cells

Human cervix carcinoma HeLa cells (ATCC) were grown in Dulbecco's modified Eagle medium (DMEM; GIBCO, Thermo Fisher Scientific, Waltham, MA) supplemented with 10% fetal calf serum and 2 mM L-glutamine, 100 U/ml penicillin, 100 g/ml streptomycin (GIBCO) in a humidified incubator in 37 °C with 5% atmospheric CO_2.

2.2 Methods

2.2.1 Preparation of Nanogels

OH-sP(EO-stat-PO) six-arm star pre-polymers, prepared by the core-first divergent approach using anionic polymerization and sorbitol initiator, were kindly provided by Dow Chemical

Company (Terneuzen, NL). Nuclear magnetic resonance (NMR) analysis of the end groups confirmed that 80% of the end groups were secondary alcohols originating from PO.

To produce isocyanate-functionalized NCO-sP(EO-stat-PO) for reactive self-assembly, isocyanate end groups were prepared by a reaction of OH-sP(EO-stat-PO) with isophorone diisocyanate (IPDI; 98%; Sigma-Aldrich, Munich, Germany). During the synthesis, the polyol was added to an 80-fold excess of IPDI and stirred for three days at 55 °C under nitrogen atmosphere. The excess of IPDI was removed by short path distillation. The product was purified by precipitation in cold diethyether.

To produce the nanogels, by either reactive non-reactive or reactive self-assembly, OH-sP(EO-stat-PO) or NCO-sP(EO-stat-PO) was dispersed in ultrapure water with concentrations ranging from 5 to 20 mg/ml and stirred overnight at room temperature. The isocyanate-functionalized star polymers (NCO-sP(EO-stat-PO)) were weighed under an inert gas and dissolved in water by stirring at different speeds ranging from 300 to 900 rpm for 24 hours.

2.2.2 Preparation of Functionalized Nanogels

The nanogels were functionalized in situ either with the TAT peptide (YGRKKRRQRRRC) or with the peptide with a random amino acid sequence (Ran, GARGEGINGC). The peptides were covalently attached to the nanogels via urea linkage. For imaging, the nanogels were labeled covalently with amine-functional Alexa Fluor 488 (Thermo Fisher Scientific). In detail, 100 mg (8,3·10-3 mmol, 1 eq) of the pre-polymer NCO-sP(EO-stat-PO) was dissolved in ultrapure water. Subsequently, 0,8 mol eq peptides and 0,1 mol eq amine functional Alexa Fluor 488 dye (Thermo Fisher Scientific) were added. The final concentration of the pre-polymer in water was 10 mg/ml. After 24 h, the nanogel dispersion was dialyzed against water for 3 days. For dialyses, a regenerated cellulose membrane (Spectra/Por 7, Spectrum Laboratories Inc., Broadwick, CA,

USA) with a molecular weight-cutoff (MWCO) of 25000 g/mol was used. Finally, pyrene was incorporated as a hydrophobic compound into the nanogels. Therefore, different amounts of a stock solution of pyrene in acetone was added to glass vials and incubated for 3 hours to evaporate the acetone. Then, the pre-polymer solution was added, and the mixture was stirred in the dark for 24 h at room temperature.

2.2.3 DLS

Particle sizes were measured by photo correlation spectroscopy using a Malvern Zetasizer Nano ZS (Malvern Instruments Ltd., Worcestershire, UK) with a 633 nm He-Ne laser. The scattered light was detected at an angle of 173,8°. The autocorrelation function was analyzed by the cumulants method. The hydrodynamic radius of the nanogels was calculated by the Stokes–Einstein equation $D=kT/3\pi\eta d$, where *D* is the diffusion coefficient, *k* the Boltzmann constant, *T* is the temperature, and η is the viscosity of the solvent.

2.2.4 Cryo-SEM and TEM

Cryo-SEM was performed with a Hitachi S-4800 microscope (Hitachi High-Technologies Corp., Tokyo, Japan). The working distance was set to 9 and accelerating voltage was 1 kV. The sample concentration was 1 mg/ml. The specimens were prepared by depositing a drop on the sample holder, followed by rapid freezing in liquid nitrogen and transfer into the high vacuum cryo unit. The tip of the specimen was cut to gain a smooth surface. To improve contrast between the nanogels and the frozen water, a thin layer of the water was sublimated for 5 minutes.

TEM was performed with a Libra 120 (Carl Zeiss, Jena, Germany) with an accelerating voltage of 120 kV. The nanogel samples (10 µl) were prepared on a silicon-coated copper grid and imaged after three days of incubation.

2.2.5 Fluorescence Spectroscopy

Measurements were performed with a LS50 spectrometer (Perkin-Elmer Ltd., Beaconsfield, United Kingdom). The spectra were recorded at an angle of 90° and slit openings of 0.5 nm. Excitation spectra were carried out at an emission wavelength of 390 nm.

2.2.6 Confocal Microscopy

For live cell imaging, cells were grown to 80% confluency on 21.5 cm^2 glass-bottom culture dishes (1.5 glass thickness, MatTek Cultureware, Ashland, MA) and then continuously transduced with the Alexa-488 conjugated nanogels with or without peptides. Timelapse imaging was performed either by CellObserver HS widefield (Carl Zeiss AG, Jena, Germany) or by laser scanning confocal microscope LSM510 (Carl Zeiss AG). Images were taken at 5 min intervals. Widefield images were captured using LD Plan-Neofluar 40x (NA=0.6) objective. Microscope incubator was maintained at 37 °C and CO_2 concentration was 5%. The LSM 510 objective and the sample holder were warmed to 37 °C prior to imaging. 3D stacks of 15–30 cross-sectional images were acquired with a Plan-Neofluar 63x oil immersion objective (NA=1.25). Image size was adjusted to 512 x 512 pixels with a X-Y resolution of 100 nm/voxel and Z of 350 - 500 nm/voxel. A 488-nm argon laser line was used for Alexa-488 excitation, and fluorescence was collected with a 520-560 nm band-pass filter.

For immunolabeling, cells were seeded on round coverslips and incubated with the Alexa-488 conjugated nanogels (1000 µg/ml) carrying TAT or the randomandom peptide. Incubation time was 15 min, 30 min, 2 h, 10 h or 24 h, after which the samples were fixed with 4% paraformaldehyde (PFA; 15 min at room temperature) and embedded with ProLong® Gold antifade reagent with or without DAPI (Thermo Fisher Scientific). Lysosomes were labeled with a monoclonal antibody (MAb) LAMP2 (Hybridoma Bank,

Iowa City, Iowa), followed by goat anti-mouse Alexa-555 conjugated secondary antibody (Ab, Thermo Fisher Scientific). In confocal microscopy (Olympus FV-1000 IX-81, Olympus, Tokyo, Japan). Alexa 488 nm was excited with a 488 nm argon laser and fluorescence was collected with a 510-540 nm band-pass filter.Alexa 555 was excited with a 543 nm He-Ne laser and fluorescence was collected with a 570-620 nm band-pass filter. Colocalization was analyzed by ImageJ using the JACoP plugin (Bolte & Cordelieres 2006).

2.2.7 Flow Cytometry

Cells were transduced with the Alexa488 conjugated nanogels with or without peptides for 2 or 24 h, detached by scraping, and washed with phosphate-buffered saline. The amount of intracellular nanogels was analyzed by FACSCalibur flow cytometer and CellQuest software (Beckton Dickinson, Heidelberg, Germany). The mean fluorescence intensity (MFI) of the cells at FITC-A channel was measured. Extracellular fluorescence was quenched with trypan blue, and untreated cells were used as controls. Means of one representative experiment were counted from quadruplicate measurements with a total of 4×10^4 cells.

3 Results and Discussion

We prepared nanogels from aqueous solutions of amphiphilic NCO-sP(EO-stat-PO) pre-polymers through reactive self-assembly (Figure 1). First, we developed a synthetic protocol allowing the self-assembly of nanogels within the size range of 100-250 nm. Next, we loaded the hydrophobic pockets of the nanogels with pyrene as a model drug molecule based on hydrophobic interaction. Finally, we used the NCO groups during nanogels formation to covalently bind fluorescence dyes and peptide sequences, randomized as well as cell penetration peptides, onto the nanogels, and studied their cellular uptake into HeLa cells.

Figure 1. Synthesis of Nanogels from NCO-sP(EO-stat-PPO). Production of chemically cross-linked hydrogel includes the introduction of reactive groups at the end of the HO-sP(EO-stat-PO) chains. Reactive polymers are then prepared by endcapping the hydroxy terminated polymer HO-sP(EO-stat-PO) with IPDI. Hydrolysis of the isocyanate groups first leads to the formation of carbamic acid and amino groups. Next, the formation of urea bridges between amino and isocyanate groups induces the synthesis of nanogels with densely cross-linked network. The yellow dots represent isocyanate end groups, and the green dots represent amine groups.

3.1 Self-assembly of Nanogels

The self-assembly of macromolecular building blocks is a versatile route for nanogel production. Several earlier studies have used amphiphilic block copolymers (Liu et al. 2016, Park et al. 2003, Ryu et al. 2010), however, only a few studies have utilized more complex star copolymers for nanogel production (Hadjichriistidi*s* et al. 2003). The unique topological structure, in combination with their physical and chemical properties, make star copolymers ideal components for the synthesis of nanogels with a well-defined polymer network. The high number of peripheral end groups of star copolymers allows the attachment of a variety of compounds such as dyes, peptides and other biomolecules. In addition, their three-dimensional globular structure facilitates the encapsulation of cargo (Wua et al 2015).

Nanogels based on nonionic PEO have many advantages for biomedical applications, such as chemical stability, water solubility, non-toxicity, and minimized recognition by the immune

system (Lapienis 2009). However, since EO homopolymers themselves do not exhibit sufficient intermolecular interaction in water to aggregate (Edwards-Gayle 2018), it is necessary to introduce hydrophobic motifs in the polyether backbone in order to trigger self-assembly. We thus employed six-arm, star-shaped polymers with a sorbitol core and a polyether backbone consisting of statistically copolymerized ethylene oxide and propylene oxide in a ratio 4:1 (sP(EO-stat-PO)) as building blocks for nanogel formation. Copolymerization of hydrophilic EO and hydrophobic PO leads to amphiphilicity of the resulting polymer (Rastogi et al. 1970). Several studies have shown that linear diblocksand triblocks of EO and PO micelles can be successfully used in drug delivery systems (Hamley 2005, Alexandridis 1997, Alexandridis 1997).

For star-shaped molecules, the higher reactivity of EO leads to a gradient distribution of PO along the backbone, with a higher PO content towards the distal endings of the star molecules. In order to prove that these molecules do aggregate in water, we examined the aggregation behavior of the OH-terminated sP(EO-stat-PO) molecules. To optimize reaction conditions, we analyzed the effect of various polyol concentrations on the size and stability of OH-sP(EO-stat-PO) polyols by DLS, cryo-SEM and TEM. The DLS measurements showed two distinct peaks (Figure 2A). The smaller peak at 6 nm indicated the presence of molecular unimers in solution with a size independent of the polyol concentration. This was in good agreement with the calculated value of the hydrodynamic radius of the particles (2.5-3.0 nm, see SI). The second peak indicated the presence of aggregates formed by clustering of the unimers (Figure 2A). Of note, the size of the aggregates (97-142 nm) correlated with the concentration (5-20 mg/ml) of the polyol. The largest, 142 nm, particles were formed when the polyol concentration was 20 mg/ml (Figure 2B, Table S1). Consistent with the DLS data, Cryo-SEM analysis showed that the particles exhibited a smooth, spherical shape with a mean diameter of 93 nm ± 13 nm (Figure 2C). Our results indicated that the number of aggregates in the solution was low in comparison to the number of unimeric micelles. This is in line with the Rayleigh equation stating that the

intensity of the scattered light of a particle is proportional to the sixth power of its diameter. Our data also demonstrated that nature of the polymer backbone is sufficiently amphiphilic for self-assembly, and that there is a equilibrium between molecular unimers and aggregates in solution. Our results are consistent with earlier studies showing that there is an equilibrium between unimers and aggregates in a solution containing 4-arm star block copolymer, sP(EO-block-PO) (Branca et al. 2002). In addition, our results are supported by studies showing that both linear block copolymers and linear gradient copolymers of EO and PO undergo self-assembly (Kelarakis et al. 2004).

Figure 2. Characterization OH-sP(EO-stat-PO) Star Polyols. (A) DLS analysis of polymer particle size in water at different polyol concentrations (5-20 mg/ml). (B) DLS analysis showing mean diameter of aggregates. Error bars represent the ± standard deviation of mean (± SD, n=5). (C) Cryo-SEM image of an aqueous polymer solution at a concentration of 1 mg/ml. Scale bar, 500 nm.

Next, we endowed the star-shaped polyether alcohols with reactive NCO end groups by end-capping the alcohol groups through a reaction with isophorone-diisocyanate (IPDI). Aside of the NCO groups, this also introduced further hydrophobicity at the distal endings of the star molecules due to the cyclohexane-based isophorone ring, and thus enhanced the amphiphilicity of the molecules (Ma et al. 2001, Herfurth et al. 2012). We then prepared nanogels by reactive self-assembly of NCO-sP(EO-stat-PO), by using the procedure described in Figure 1. The DLS analysis showed, in contrast to non-reactive self-assembly, the presence of one peak, suggesting a relatively unimodal and narrow size distribution. The absence of the unimer peak indicated that all unimers assembled into nanogels as a consequence of the enhanced amphiphilicity and the water-induced chemical cross-linking (Figure 3A). The produced nanogels were monodisperse with a hydrodynamic radius of 111-207 nm. The hydrodynamic radius of the particles correlated with the concentration of the polymers (Figure 3B, Table S2). Cryo-SEM image analyses indicated that the nanogels had a mean diameter of 126 ± 11 nm (Figure 3C). The diameter

measured was similar to the DLS data of nanogels produced at the concentration of 10 mg/l. The nanogels from reactive self-assembly were slightly larger than those from non-reactive self-assembly for all concentrations examined (Tables S1 and S2). This originates from the fact that all molecules participate in the nanogel formation due to the enhanced driving force for aggregation and the subsequent chemical cross-linking between the isocyanate end groups through their hydrolysis to amines and the following formation of urea bridges.

Figure 3. Characterization of NCO-sP(EO-stat-PO) Polyether Nanogels. (A) DLS analysis of nanogel diameter in water at different polyol concentrations (5-20 mg/ml). (B) Influence of polyether concentration on the size. Error bars represent the ± SD, n=5. (C) Cryo-SEM images of the nanogels. The sample was prepared with a concentration of 10 mg/ml. Scale bar, 500 nm.

To verify reproducibility, particle preparation by non-reactive and reactive self-assembly was carried out five times under the same conditions. The measurements indicated that both syntheses were reliable and reproducible. Additionally, the impact of preparation conditions on particle formation and robustness was investigated by employing different synthesis parameters. Stirring rates of 100-800 rpm had no effect on the particle size, whereas shearing effects caused by rates higher than 900 rpm inhibited particle formation.

We then compared the stability of the physical sP(EO-stat-PO) aggregates and the chemically cross-linked NCO-sP(EO-stat-PO) derived nanogels over time and also against dilution using DLS for characterization. Within 2 weeks of storage, the sP(EO-stat-PO) solution constantly exhibited 2 peaks, unimers and aggregates, and the aggregates showed size variations within the range of the standard deviation. This underlines a dynamic equilibrium between unimeric micelles and aggregates. In comparison, the diameter of the NCO-sP(EO-stat-PO) nanogels remained constant for over 4 months, and no unimer peak occurred over time, underlining stability of the systems due to the chemical cross-linking (Table S3). Additionally, DLS analyses of dilution stability showed that the diameter of NCO-sP(EO-stat-PO) nanogels remained constant with no unimers detaching upon dilution (Table S4). Taken together, the preparation of

nanogels by reactive self-assembly is a robust method, and reproducibly results in constant-sized and long-term storage stable particles.

3.2 Evaluation of Loading with Hydrophobic Molecules

The possibility to load the nanogels with hydrophobic molecules based on non-covalent physical interaction was investigated by fluorescence spectroscopy using pyrene as a model compound. Pyrene is a fluorescent hydrophobic dye with certain solubility in water and a fluorescent spectrum that shows a solvatochromic effect. The migration of a pyrene molecule from a hydrophilic to a hydrophobic region induces a red shift of the adsorption band accompanied by enhanced intensity (Kalyanasundaram et al. 1997). Here, analyses of the nanogels polymerized in the presence of pyrene indicated a shift of the peak in the excitation spectra (Figure 4). The red shift of the peak from 334,5 nm to 337,0 nm showed the incorporation of pyrene in the hydrophobic domains of the nanogels. In parallel, the fluorescence intensity of pyrene inside the nanogels increased up to 10 times in comparison to pyrene in the hydrophilic control solution. Together with the shift in wavelength, this indicates that the pyrene molecules were shielded from water in hydrophobic domains of the nanogels. Hence, our results demonstrate that these nanogels can be loaded with hydrophobic guest molecules.

Figure 4. Excitation Spectra of Pyrene Detected at an Emission Wavelength of λ_{em} = 390 nm. The black curve represents pyrene dissolved in water. The other spectra show curves from pyrene incorporated into nanogels of various sizes.

3.3 Cellular Uptake

For biomedical applications, the interaction between the nanogels and living cells is crucial. We have demonstrated earlier that hydrogels prepared from NCO-sP(EO-stat-PO) prepolymers are cytocompatible and that such gels, if implanted subcutaneously into mice, do not cause negative effects, neither in the tissue surrounding the gels nor systemically (Neuerburg et al. 2013). Here,

to understand the nanogel-cell interactions, we first assessed the cellular uptake of non-functionalized fluorescent nanogels into HeLa cells by confocal fluorescence microscopy. These studies indicated that only a trace amount of nanoparticles were located in the cells at 24 h post transduction (p.t.) (Figure 5A). This demonstrates that the nanogels, as colloidal and soft hydrophilic polymer networks with a high water content and without a primary phase boundary, are not recognized by the cells and thus not internalized. Next, we produced peptide-functionalized nanogels and followed their cellular entry. To preferentially bind the peptide N-terminus to icocyanates, we used peptide sequences with N-terminal cysteine. Thus, both the thiol group and the N-terminal amine group would be presented adjacently. As a proof of principle, the non-specific but highly efficient and well-known, cell penetration peptide sequence TAT was used. To assure that the attachment of peptides as such does not alter the nanogel behavior, we also functionalized nanogels with a random peptide sequence of equal length. Confocal imaging of fixed cells showed that the nanogels with TAT peptide entered the cell cytoplasm at 2 h p.t. The time-dependent increase in intracellular TAT-modified nanogels, and their localization into vesicular-like structures in the nuclear periphery was detected at 24 h p.t. (Figure 5B). In contrast, only a small portion of the nanogels with the control peptide, similarly to non-functionalized nanogels, was detected in the cytoplasm either at 2 or 24 h p.t. (Figure 5C). This indicates that the cellular entry of nanogels was controlled and directed by the TAT peptide.

Figure 5. Intracellular Entry of Nanogels. Confocal microscopy images of intracellular distribution of Alexa-488 conjugated nanogels (green) at 2 and 24 h p.t. Localization of nanogels (A) without peptide, (B) with TAT and (C) random (Ran) peptide with DAPI (blue) are shown. Both differential interference contrast images (DIC) and pseudocolor images with intensity increasing from black to white were used to visualize the intracellular distribution of nanogels. The transduction concentration of nanogels was 1000 μg/ml. Scale bars, 10 μm.

The timing of cell entry of the TAT-conjugated nanogels was analyzed by time-lapse imaging. Imaging of cells at 5 min p.t. showed that the TAT-nanogels were located in a circular region along the cellular rim either inside or outside the cytoplasm. At around 80 min and more clearly at 2 h p.t., the presence of nanogels in the cytoplasm was detected. Their amount in the cytoplasm increased time-dependently and within 12 hours most of the cells had them internalized. The amount of intracellular TAT-nanogels increased until 24 h p.t. Consistently with fixed cell studies (Figure 5), the number of vesicular structures containing TAT-nanogels was highest at the nuclear periphery.

Figure 6. Internalization of Nanogels in Living Cells. Time-lapse images of nanogels with TAT peptide and Alexa-488 at 5 min, 12 and 24 h p.t. (1 mg/ml). Pseudocolor coloring demonstrates the distribution of fluorescence intensity depending on the intracellular amount of nanogels. See also Supplementary movie S1.

The time-lapse imaging revealed that cells with internalized TAT-nanogels continued to undergo cell division (Movie 1). This suggests that the TAT-nanogels, produced from biocompatible polyethylene glycol, elicit no cytotoxic effect on cell growth at the concentration of 1 mg/ml. Confocal studies confirmed that the rate of cell death compared with control cells did not increase even after 24 h p.t. Analyses of nuclear morphology and chromatin distribution in DAPI-labeled cells indicated no signs of apoptosis, including chromatin condensation and nuclear fragmentation (Kepp et al. 2011). This is in line with earlier studies showing that the nanogels synthesized by cross-linking self-assembling polymers possess low cytotoxicity (Chacko et al. 2012). These results indicate that the nanogels produced in our study are nontoxic and thus potential candidates for biological applications.

To determine how nanogel concentration and the time elapsed affect the cellular uptake of nanogels, cells were transduced with 10, 100, and 1000 µg/ml of Alexa488 conjugated nanogels

either without peptide, with TAT peptide or with the random peptide, and intracellular fluorescence signal was analyzed by flow cytometry at 2 and 24 h p.t. In general, our results indicated that the highest fluorescence corresponding to the amount of intracellular nanogels was detected in 1000 µg/ml transduced cell both at 2 and 24 h p.t. (Figure 7). At 2 h p.t. only a minute amount of nanogels (without peptide / TAT / random peptide), were internalized after transduction with 10 and 100 µg/ml. The cells transduced with 1000 µg/ml showed relatively similar cellular fluorescences for without peptide, TAT, and the random peptide (5.3 ± 1.7, 6.7 ± 1.3, 4.9 ± 1.5) at 2 h p.t. Of note, the amount of uptake of TAT peptide conjugated nanogels was significantly ($p < 0.01$) increased at 24 h p.t. in cell transduced with 100 and 1000 µg/ml (10.3 ± 1.6, 57.3± 7.4) in comparison to the uptake of nanogels without peptide and with the random peptide (3.4 ± 0.08, 22.8 ± 0,8; 2.4 ± 0.03, 15.0 ± 0.6). This indicates that at a concentration of 1000 µg/ml, the cellular uptake of the nanogels with TAT peptide was 3,8-fold higher than the uptake of the nanogels with the randompeptide, and 2,5-fold higher than the uptake of the nanogels without a peptide. Taken together, TAT peptide was able to significantly facilitate the cellular uptake of the nanogels in a concentration and time-dependent manner.

Figure 7. Assessment of Cellular Uptake of Nanogels as Function of Concentration and Time. Flow cytometry analysis of cells transduced with 0.01, 0.1, and 1 mg/ml of Alexa -488 nanogels with TAT (TAT, orange) or random peptide (Ran, brown), and without peptide (without, yellow) at 2 and 24 h p.t. Untreated cells were used as controls with signal set to 1 (not shown). The mean values ± SD are shown.

Finally, we hypothesized, in line with earlier studies, that the nanoparticles with TAT peptide enter the cells mainly by an endocytic pathway ending up in lysomal vesicles (Rinne et al. 2007, Abes et al. 2006, Jones et al. 2007). To test this hypothesis, we analyzed the subcellular localization of the nanogels with TAT peptide (1 mg/ml) and the lysosome marker LAMP-2. Our results showed that at 10 and 24 h p.t the nanogels and lysosomes were frequently found in similar locations in the nuclear periphery (Figures 8A and 8B). Quantitative co-localization

analysis indicated an increasing colocalization of the nanogels with the lysosomal marker after 30 min (42 ± 0.9 %) pt. The colocalization further increased at 2 h p.t. (80 ± 0.8 %), and was highest at 24 h p.t. (90 ± 0.8) (Figure 8C, Supporting information Figure SI). The observation of minor colocalization at 0 and 15 min p.t. could be explained by unspecific binding of the antibody to nanogel-containing pericellular structures.

Figure 8. Intracellular Distribution of Nanogels and Lysosomal marker. (A) Confocal microscopy images of cells transduced with Alexa -488 labeled nanogels conjugated with TAT peptide (green, 1 mg/ml). The cells were fixed at 24 h p.t. and labeled with LAMP2 MAb (red) and DAPI (blue). Scale bars, 10 µm. (B) Quantitative analyses showing the percentage of nanogel and LAMP2 MAb colocalization at various time points.

In summary, these results verified that nanogels functionalized with TAT were able to enter and accumulate in a human cancer cell line. Moreover, our data suggest that during their cellular entry, the nanogels use endocytic pathway for internalization, followed by their accumulation into lysosomes in the nuclear periphery. These findings are consistent with earlier studies, which showed that TAT peptide and TAT-conjugated nanoparticles enter the cells either via clathrin-mediated endocytosis or macropinocytosis, and end up in lysosomes, the last compartment on the endocytic pathway.

4 Conclusions

In this study, we prepared nanogels through reactive self-assembly of isocyanate functional amphiphilic six-arm star-shaped prepolymers with a backbone consisting of ethylene oxide and propylene oxide in a ratio of 4:1 (NCO-sP(EO-stat-PO). The end-capping of the hydroxy-terminated pre-polymer with isocyanate end groups enabled the synthesis of densely crosslinked nanogels, which were, unlike the bare hydroxyl-terminated polymers, stable upon dilution and

long-term storage. The size of the spherical and smooth nanogels, ranging from 116 nm to 205 nm, was controlled by the concentration of the pre-polymer. Additionally, the incorporation of pyrene as a hydrophobic model compound into hydrophobic pockets of the nanogels was demonstrated. We also showed that cellular uptake of unmodified nanogels by HeLa cells is negligible over 24 h, and that covalent attachment of a random peptide sequence does not affect this behavior. In contrast, modification of the nanogels with TAT peptide led to rapid and efficient cellular entry of the nanogels, and resulted in their enrichment in the nuclear periphery in a time and concentration-dependent manner. Taken together, we demonstrated that the production of nanogels by self-assembly and crosslinking provides a powerful approach to the creation of nanogels for biomedical applications.

Acknowledgements

The project was financed by the Jane and Aatos Erkko Foundation (MVR); the Academy of Finland, under the award number 138388 (MVR); EU FP6 project “3g-Nanotechnology based targeted drug delivery using the inner ear as a model target organ (NanoEar)”, project ID 26556 (MVR, JG).

Conflict of Interest

The authors declare no conflict of interest.

4.5 References

Hamidi, M., Azadi, A., Rafiei, P., *Adv. Drug Deliv. Rev.*, 2008, *60*, 1638-1649.

Oh, J. K., *Can. J. Chem*., 2010, *88*, 173-184.

Kabanov, A. V., Vinogradov, S. V., *Angew. Chem. Int. Ed*., 2009, *48*, 2-14.

Vinogradov, S. V., Batrakova, E. V., Kabanov, A. V., *Colloids Surf. B. Biointerfaces*, 1999, *16*, 291-304.

Yallapu, M. M., Jaggi, M., Chauhan, S. C., *Drug Discovery Today*, 2011, *16*, 9-10, 457-463.

Li, Y., Maciel, D., Rodrigues, J., Shi, X., Tomás, H., *Chem. Rev.*, 2015, *115*, 8564-8608.

Wu H-Q and Chang-Chun Wang. Biodegradable Smart Nanogels: A New Platform for Targeting Drug Delivery and Biomedical Diagnostics. *Langmuir*, 2016, 32 (25), pp 6211–6225.

Chen W, Nathaniel B. Zuckerman, James W. Lewis, Joseph P. Konopelski and Shaowei Chen. Pyrene-Functionalized Ruthenium Nanoparticles: Novel Fluorescence Characteristics from Intraparticle Extended Conjugation. *J. Phys. Chem. C*, 2009, 113 (39), pp 16988–16995.

Salvador-Morales, C., Zhang, L., Langer, R., Farokhzad, O. C., *Biomaterials*, 2009, *30*, 2231-2240.

Gratton, S. E., Ropp, P. A., Pohlhaus, P. D., Luft, J. C., Madden, V. J., Napier, M. E., DeSimone, J. M., *Proc. Natl. Acad. Sci. U.S.A.*, 2008, *105*, 11613-11618.

Bertrand N, Philippe Grenier, Morteza Mahmoudi, Eliana M. Lima, Eric A. Appel, Flavio Dormont, Jong-Min Lim, Rohit Karnik, Robert Langer & OC Farokhzad. Mechanistic understanding of in vivo protein corona formation on polymeric nanoparticles and impact on pharmacokinetics. Nature Communications 8(1): 777 (2017).

Jarver P, U Langel: The use of cell-penetrating peptides as a tool for gene regulation.Drug Discov Today 2004, 9:395-402.

Field LD, James B. Delehanty, YungChia Chen, and Igor L. Medintz, Peptides for Specifically Targeting Nanoparticles to Cellular Organelles: Quo Vadis?, Acc. Chem. Res., 2015, 48 (5), pp 1380–1390.

Petros, R. A., DeSimone, J. M., Strategies in the design of nanoparticles for therapeutic applications. Nat. Rev. Drug Discovery, 2010, 9, 615-627.

Vasir JK, Reddy MK, Labhasetwar V. Nanosystems in drug. targeting: opportunities and challenges. Curr Nanosci 2005; 1: 47-64.

Krsko P, Libera M. Biointeractive hydrogels [J]. Materials Today, 2005, 8(12): 36–44.

Lewin, M.; Carlesso, N.; Tung, C. H.; Tang, X. W.; Cory, D.; Scadden, D. T.; Weissleder, R. Tat peptide-derivatized magnetic nanoparticles allow in vivo tracking and recovery of progenitor cells. Nat. Biotechnol. 2000, 18, 410−414.

Nitin Nitin, Leslie LaConte, Won Jong Rhee, and Gang Bao. Tat Peptide Is Capable of Importing Large Nanoparticles Across Nuclear Membrane in Digitonin Permeabilized Cells, Ann Biomed Eng. 2009 Oct; 37(10): 2018–2027.

Pan L, Qianjun He, Jianan Liu, Yu Chen, Ming Ma, Linlin Zhang, and Jianlin Shi, Nuclear-Targeted Drug Delivery of TAT Peptide-Conjugated Monodisperse Mesoporous Silica Nanoparticles J. Am. Chem. Soc., 2012, 134 (13), pp 5722–5725.

Roosmarijn E. Vandenbroucke , Stefaan C. De Smedt , Joseph Demeester , Niek N. Sanders. Cellular entry pathway and gene transfer capacity of TAT-modified lipoplexes. Biochimica et Biophysica Acta (BBA) - Biomembranes 2007 1768, 571-579.

Mann DA, AD Frankel: Endocytosis and targeting of exogenous HIV-1 Tat protein. EMBO J 1991, 10:1733-9.

Richard P, K. Melikov, H. Brooks, et al. .Cellular uptake of unconjugated TAT peptide involves clathrin-dependent endocytosis and heparan sulfate receptors. J Biol Chem, 280 (2005), pp. 15300-1530

Kaplan, J.S. Wadia, S.F. DowdyC. Cationic TAT peptide transduction domain enters cells by macropinocytosisJ. Controlled Release, 102 (2005), pp. 247-25.

Choi HS, Liu WH, Misra P, Tanaka E, Zimmer JP, Ipe BI, Bawendi MG, Frangioni JV. Renal clearance of quantum dots. Nat. Biotechnol. 2007;25:1165–1170.

Rastogi, A. K., Pierre, L. E., Copolymerization of ethylene oxide and propylene oxide by anhydrous potassium hydroxide. J. Appl. Polym. Sci., 1970, 14, 1179-1182.

Bolte S, Cordelieres FP. 2006). A guided tour into subcellular colocalisation analysis in light microscopy. J Microsc 224:13–232.

Liu JC, Uhlir C, Shah PK, Sun F, Stansbury JW. Controlled nanogel and macrogel structures from self-assembly of a stimuli-responsive amphiphilic block copolymer. RSC Advances 2016 6 (69), 64791-6479

Park C, Yoon J, Thomas EL. Enabling nanotechnology with self assembled block copolymer patterns. Polymer. 2003;44:6725–60.

Hadjichriistidi*s* N., Pitsikalis M., Iatrou H., Driva P., Sakellariou G., Chatzichristidi M. Polymers with Star-Related Structures*:* Synthesis, Properties and Applications*"*, Volume 6*:* Macromolecular Architectures and Soft Nano-Objects, Polymer Science: A Comprehensive Reference, *2012*, pages *29-111*.

Wua W, Weigang Wanga, Jianshu Li. Star polymers: Advances in biomedical applications. Progress in Polymer Science 46 (2015) 55–85.

Hamley, IW. Block Copolymers in Solution: Fundamentals and Applications, Wiley, 2005.

Alexandridis, P., Holzwarth, J. E, Hatton, T. A. Macromolecules 1994, 27, 2414

Alexandridis, P. Curr. Opin. Colloid Interface Sci. 1997, 2, 478-489.

Branca C, S.Magazu, F.Migliardo. Star polymer/water solutions: new experimental findings. Condensed Matter Physics, 2002, Vol. 5, No. 2(30), pp. 275–284.

Kelarakis A, Shao-Min Mai, Vasiliki Havredaki, Alison Brett, and Colin Booth. Thermodynamics of micellization of tapered statistical copolymers of ethylene oxide and propylene oxide in water. Journal of Colloid and Interface Science 275 (2004) 439–444.

Ma SX, Cooper SL. Shear Thickening in Aqueous Solutions of Hydrocarbon End-Capped Poly(ethylene oxide). Macromolecules 2001, 34, 3294-3301.

Herfurth C, Paula Malo de Molina, Christoph Wieland, Sarah Rogers, Michael Gradzielski and André Laschewsky. One-step RAFT synthesis of well-defined amphiphilic star polymers and their self-assembly in aqueous solution. Polym. Chem., 2012, 3, 1606-1617.

Kalyanasundaram K, J. K. Thomas, Environmental effects on vibronic band intensities in pyrene monomer fluorescence and their application in studies of micellar systems. J. Am. Chem. Soc., 1977, *99*, 2039-2044.

Kepp O, Lorenzo Galluzzi, Marta Lipinski, Junying Yuan & Guido Kroemer. Cell death assays for drug discovery. Nature Reviews Drug Discovery 2011 10, 221-237.

Chacko, RT, Ventura J, Zhuang J, Thayumanavan S. Polymer nanogels: a versatile nanoscopic drug delivery platform. Adv Drug deliv Rev, 2012 15;64(9): 836-851.

Rinne J, Albarran B, Jylhävä J, Ihalainen TO, Kankaanpää P, Hytönen VP, Stayton P, Kulomaa MS, and Vihinen-Ranta M (2007). Internalization of novel TAT-Streptavidin Fusion Protein In Mammalian Cells. BMC Biotechnol. 2;7(1):1.

Abes, S.; Williams, D.; Prevot, P.; Thierry, A.; Gait, M.J.; Lebleu, B. Endosome trapping limits the efficiency of splicing correction by PNA-oligolysine conjugates. J. Control. Release 2006, 110, 595–604.

Jones, A.T. Macropinocytosis: searching for an endocytic identity and role in the uptake of cell penetrating peptides. J. Cell. Mol. Med. 2007, 11, 670–684.

F. Topuz, S. Singh, K. Albrecht, M. Moeller, J. Groll: DNA Nanogels Snare Carcinogens: A Bioinspired Generic Concept with High Efficiency. Angewandte Chemie International Edition 2016, 55(40), 12210-12213.

M. J. Kettel, K. Schaefer, J. Groll, M. Moeller: Nanogels with high active ß-cyclodextrin content as physical coating system with sustained release properties.
ACS Applied Interfaces 2014, 6, 2300−2311.

M. J. Kettel, H. Hildebrandt, K. Schaefer, M. Moeller, J. Groll: Tenside Free Preparation of Nanogels with High Functional β-Cyclodextrin Content.
ACS Nano 2012, 6(9), 8087–8093.

Ja-Hyoung Ryu, Siriporn Jiwpanich, Reuben Chacko, Sean Bickerton, and S. Thayumanavan: Surface-Functionalizable Polymer Nanogels with Facile Hydrophobic Guest Encapsulation Capabilities.
J. AM. CHEM. SOC. 2010, 132, 8246–8247.

C. Neuerburg, S. Recknagel, J. Fiedler, **J. Groll**, M. Moeller, K. Bruellhoff, H. Reichel, A. Ignatius, R. E. Brenner: Ultrathin sP(EO-stat-PO) hydrogel coatings are biocompatible and preserve functionality of surface bound growth factors in vivo.
Journal of Materials Science: Materials in Medicine 2013, 24(10), 2417-27.